Journal of Materials Science: Materials in Medicine (2019) 30:1
https://doi.org/10.1007/s10856-018-6202-x

TISSUE ENGINEERING CONSTRUCTS AND CELL SUBSTRATES

Original Research

3D-porous β-tricalcium phosphate–alginate–gelatin scaffold with DMOG delivery promotes angiogenesis and bone formation in rat calvarial defects

Shahrbanoo Jahangir[1,2] · Samaneh Hosseini[1] · Farhad Mostafaei[3] · Forough Azam Sayahpour[1] · Mohamadreza Baghaban Eslaminejad[1]

Received: 30 June 2018 / Accepted: 6 December 2018 / Published online: 18 December 2018

Abstract

Hypoxia-inducible factor-1α (HIF-1α), a well-studied angiogenesis pathway, plays an essential role in angiogenesis-osteogenesis coupling. Targeting the HIF-1a pathway frequently leads to successful reconstruction of large-sized bone defects through promotion of angiogenesis. Dimethyloxalylglycine (DMOG) small molecule regulates the stability of HIF-1α at normal oxygen tension by mimicking hypoxia, which subsequently accelerates angiogenesis. The current study aims to develop a novel construct by seeding adipose derived mesenchymal stem cells (ADMSCs) onto a scaffold that contains DMOG to induce angiogenesis and regeneration of a critical size calvarial defect in a rat model. The spongy scaffolds have been synthesized in the presence and absence of DMOG and analyzed in terms of morphology, porosity, pore size, mechanical properties and DMOG release profile. The effect of DMOG delivery on cellular behaviors of adhesion, viability, osteogenic differentiation, and angiogenesis were subsequently evaluated under in vitro conditions. Histological analysis of cell-scaffold constructs were also performed following transplantation into the calvarial defect. Physical characteristics of fabricated scaffolds confirmed higher mechanical strength and surface roughness of DMOG-loaded scaffolds. Scanning electron microscopy (SEM) images and MTT assay demonstrated the attachment and viability of ADMSCs in the presence of DMOG, respectively. Osteogenic activity of ADMSCs that included alkaline phosphatase (ALP) activity and calcium deposition significantly increased in the DMOG-loaded scaffold. Computed tomography (CT) imaging combined with histomorphometry and immunohistochemistry analysis showed enhanced bone formation and angiogenesis in the DMOG-loaded scaffolds. Therefore, spongy scaffolds that contained DMOG and had angiogenesis ability could be utilized to enhance bone regeneration of large-sized bone defects.

Supplementary information The online version of this article (https://doi.org/10.1007/s10856-018-6202-x) contains supplementary material, which is available to authorized users.

✉ Mohamadreza Baghaban Eslaminejad
eslami@royaninstitute.org

[1] Department of Stem Cells and Developmental Biology, Cell Science Research Center, Royan Institute for Stem Cell Biology and Technology, ACECR, Tehran 1665659911, Iran

[2] Department of Tissue engineering & Regenerative Medicine, Faculty of Advanced Technologies in Medicine, Iran University of Medical Sciences, Tehran, Iran

[3] Animal Core Facility, Reproductive Biomedicine Research Center, Royan Institute for Biotechnology, ACECR, Tehran 1665659911, Iran

Graphical Abstract

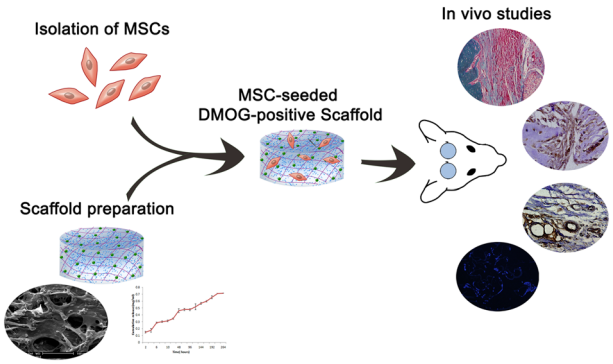

1 Introduction

Bone defects constitute one of the major global health issues that are traditionally treated with autologous or allogeneic bone grafts [1]. Major complications associated with autografts and allografts include inadequate tissue, traumatic injury, and surgical risks of hemorrhage, infection and chronic pain. Therefore, it is essential to develop a proper alternative therapeutic approach [1, 2]. The cell-loaded scaffold strategy used in tissue engineering (TE) has been developed to treat various types of bone lesions. However, limited vascular supply and accessibility to nutrients are challenges with this strategy [3].

Formation of initial blood vessels within the scaffolds and their connection with host vasculature (angiogenesis) supposedly accelerate bone tissue repair and assure the success rate of bone TE [4]. To date, various approaches (e.g., mechanobiology and growth factor delivery) have been employed to form vascular network in the constructs. Delivery of exogenous angiogenic factors such as VEGF in tissue engineered constructs are extensively used to control angiogenesis [5–7]. The complicated spatial and temporal release patterns of angiogenic factors and uncontrolled local delivery of single or even multiple growth factors result in the formation of an immature vascular network [8, 9]. In addition, high cost and degradation rate are other shortcomings associated with growth factors. An appealing approach to deal with this challenge would be to target the angiogenesis pathways and stimulate expression of angiogenic factors.

Hypoxia-inducible factor-1α (HIF-1α) is a well-recognized pathway that regulates angiogenesis-osteogenesis coupling during bone formation and the regeneration process [10]. Recent studies have shown that chondrocytes, osteoblasts, and mesenchymal stem cells (MSCs) adopt hypoxic conditions via the HIF pathway [11]. HIF-1 is a heterodimer protein composed of two subunits, HIF-1α and HIF-1β. Dimerization of these two subunits under hypoxic condition leads to transcription of angiogenic genes [12, 13]. Under normoxic conditions, two conserved proline residues of HIF-α undergo post-translational hydroxylation followed by ubiquitination that eventually causes proteasomal degradation of HIF-1α. Prolyl hydroxylases (PH) and von Hippel-Lindau (pVHL) mediate hydroxylation and ubiquitination of proline residues of the HIF-1α protein, respectively [14]. PH requires several cofactors such as iron, oxygen, and 2-oxoglutarate to fulfill the hydroxylation process [15]. Therefore, small molecules with the concept of mimicking the hypoxia condition stabilize HIF-1α and subsequently activate angiogenesis.

According to several studies, oxoglutarate analogues have the ability to stabilize HIFs and produce their beneficial biological outcome [16]. Dimethyloxalylglycine (DMOG) is a cell penetrating small molecule that inhibits PH by mimicking 2-oxoglutarate cofactors and results in the preservation of HIF-1α under normal oxygen pressure [17]. Peng et al. prohibited ovariectomy (OVX)-induced bone loss in C57BL/6J mice after treatment by DMOG, which was associated with activated HIF-1α and Wnt/beta-catenin signaling pathways [18]. Vogel et al. found that DMOG treatment of HeLa cells or prolyl hydroxylase domain (PHD)-knockout HeLa cells activated RhoA/ROCK signaling independent of HIF by inhibiting PHD [19]. More recently, the synergistic effect of DMOG and recombinant human bone morphogenetic protein-2 (rhBMP-2) was explored by Qi et al. in order to improve bone regeneration and vascular formation of a critical-sized bone defect in a rat model [20]. Although much research has been devoted to the application of DMOG for angiogenesis, there has been little investigation of DMOG in the three dimensional (3D) scaffold for angiogenesis and osteogenesis.

Selection of proper cell sources may also affect the clinical efficacy of engineered tissue. Apart from

availability, feasible harvesting, and post-transplant cell immunity, cells must have the capability to simultaneously direct both angiogenesis and osteogenesis processes [21]. Use of angiogenic cell sources could promote angiogenesis in engineered tissue. Human umbilical vein endothelial cells (HUVECs) and endothelial progenitor cells (EPCs) have been used alone or in a co-culture system to stimulate neovascularization [22]. For example, Koob et al. investigated co-implantation of HUVECs and MSCs, and attained higher neo-vessel formation without improved bone regeneration [23]. These studies successfully generated a vascularized construct, though the heterogeneity of the endothelial cells (ECs) in structure and function as well as difficulty in autologous-cell harvesting hindered their extensive use. Several studies have highlighted the role of adipose derived mesenchymal stem cells (ADMSCs) as proper cell sources for TE [24]. ADMSCs render a heterogeneous MSCs source that consists of ECs, which make it appropriate for both angiogenesis and osteogenesis [25, 26].

In this study, we aimed to fabricate an alginate-gelatin-tricalcium phosphate spongy scaffold and deliver the DMOG small molecule. We attempted to achieve enhanced loading efficiency of DMOG and a prolonged release pattern. The influence of DMOG delivery with an alginate-gelatin-tricalcium phosphate spongy scaffold was shown by the osteogenic and angiogenic potential of ADMSCs and its bone restorative ability in the treatment of critical-sized calvarial defects in rats.

2 Materials and methods

2.1 Scaffold preparation

We fabricated a spongy scaffold that included sodium alginate-gelatin-β-tricalcium phosphate according to a previously described protocol [27]. Briefly, a 1.6% (w/v) sodium alginate solution was prepared in distilled water using a magnetic stirrer, followed by the addition of gelatin powder to achieve a final concentration of 1.6%. The solution was mixed thoroughly at 50 °C. We added 0.8% (w/v) β-tricalcium phosphate in distilled water to the alginate-gelatin. To prepare the DMOG-containing scaffold, we added 1 mg/ml of DMOG in the alginate-gelatin-β-tricalcium phosphate solution. Glutaraldehyde and calcium chloride were finally added to the chemically cross-link gelatin and alginate, respectively. The solution was cast into the molds (5 mm diameter × 2 mm thick), incubated at −20 °C for 24 h, and finally freeze-dried for further experiments. Three independent samples were analyzed in all experiments.

2.2 Measurement of scaffold porosity

The porosity of the scaffold was measured by the fluid replacement method. Briefly, the scaffolds were immersed in an initial volume of ethanol (V1) in a graduated cylinder and incubated for 2 h in ethanol at room temperature. After we removed the scaffolds, we considered the remaining volume of ethanol to be V3. The percentage of porosity was calculated according to the following equation where V2 was the total volume of ethanol and the scaffolds.

$$E = \frac{(V_1 - V_3)}{V_2 - V_3} \times 100$$

We used scanning electron microscopy (SEM) images to calculate the average pore sizes for 10 different pores in each scaffold according to Image-Pro® Plus version 6.0 (Media Cybernetics, Silver Spring, MD, USA).

2.3 Mechanical properties

A compression test for the specimen (cylindrical disc: 6 mm diameter × 12 mm thick) was performed using a Santam Machine controller (version 4.24). A crosshead speed of 5 mm/min was set. Axial force and axial displacement were recorded and converted to stress and strain using the dimensions of the individual samples. Three independent samples were tested for each group.

2.4 Release pattern of dimethyloxalylglycine (DMOG)

In vitro release of DMOG from the scaffolds was carried out at 37 °C in a phosphate buffer saline (PBS) solution. The scaffolds were immersed in 1 ml PBS and the release medium was collected at pre-determined time points. The concentration of DMOG was determined by a Thermo Scientific™ Multiskan™ GO Microplate Spectrophotometer (Thermo Scientific™, USA) at a wavelength of 230 nm. The same volume of PBS was added to maintain the original volume of the PBS solution.

2.5 Adipose derived mesenchymal stem cell (ADMSC) isolation and characterization

Abdominal adipose tissue was isolated from three Wistar rat of 250 g average body weigth. The adipose tissue was cut into small pieces by a sterile scalpel, then digested by collagenase type I (1 mg/ml) and incubated at 37 °C for 30 min. The digested tissue was centrifuged at 1200 rpm for 5 min. The pellet was cultured in Dulbecco's Modified Eagle Medium (DMEM; Gibco) supplemented with 15% FBS, 1% penicillin/streptomycin, and incubated at 37 °C in 5%

CO_2. The media was changed twice weekly. We used passage-3 cells for all experiments. Isolated cells were also evaluated for their ability to differentiate into osteoblasts and adipocytes. For osteogenic differentiation, ADMSCs were incubated in osteogenic culture medium (DMEM supplemented with 10% FBS, 10 mM β- glycerophosphate, 0.2 mM ascorbic acid, and 1 nM dexamethasone) for 21 days. Osteogenesis was examined by 1% alizarin red staining. Adipogenic differentiation was induced by incubating ADMSCs in adipogenic induction medium (DMEM with 10% FBS, 0.5 mM indomethacin, 1 mM ascorbic acid, and 1 μM dexamethasone) for 21 days. We visualized lipid droplets in the cells after staining with 0.4% oil red O (data not shown). Three independent replicate ($n = 3$) were used for all experiments.

2.6 Cell viability

The 3-(4,5-dimethylthiazol-2-yl)-2,5-diphenyltetrazolium bromide (MTT) assay was indirectly performed to assess cytotoxicity of DMOG in the fabricated scaffolds. Briefly, 5×10^4 cells were seeded in a 12-well tissue culture plate. The scaffolds were placed into the cell culture insert and incubated at 37 °C. Wells without the scaffolds were considered as the control. At various time points, we removed the scaffolds and the cells were incubated in 0.5% MTT for 3 h at 37 °C. The MTT solution was removed and we added dimethyl sulfoxide (DMSO) to dissolve the formazan crystals. Optical density (OD) was measured using a Thermo Scientific™ Multiskan™ GO Microplate Spectrophotometer (Thermo Scientific™, USA) at 540 nm.

2.7 Cell seeding onto the scaffolds

First, we sterilized the scaffolds with 70% ethanol, washed them with PBS, and placed the scaffolds into 24-well tissue culture plates. Next, 1×10^6 cells were passively seeded onto the scaffolds, followed by incubation in osteogenic induction media that consisted of DMEM supplemented with 50 mg/ml ascorbic acid 2-phosphate (Sigma, USA), 10 nM dexamethasone (Sigma, USA), and 10 mM β glycerol phosphate (Sigma, USA).

2.8 Cell attachment

We evaluated the ability of ADMSCs to adhere to the scaffolds after 7 days. Cell-seeded scaffolds were fixed in 2.5% glutaraldehyde for 2 h, then washed with 0.1 M cacodylate buffer, and immersed in 1% osmium tetroxide for 2 h. Subsequently, samples were dehydrated in a graded ethanol series (30, 50, 70, 80, 90, and 100%) for approximately 20 min. The samples were subsequently coated with gold, and we assessed the morphological characteristics of the attached cells by SEM (FEI Quanta 250, Hillsboro, OR, USA).

2.9 In vitro osteogenic activities

The osteogenic property of the fabricated scaffold was evaluated in terms of ALP activity and calcium content at different time points (7 and 14 days). Alkaline phosphatase (ALP) activity was assessed using an Alkaline Phosphatase Assay Kit (Colorimetric, Abcam, USA, ab83369) according the manufacture's protocol. Briefly, cells were seeded onto the scaffolds at a density of 1×10^6 cells per scaffold. The cell-scaffold constructs were washed with PBS and lysis buffer solution was added to lyse the attached cells. After sonication and centrifugation, the cell lysis solution was analyzed for ALP activity with respect to the release of p-nitrophenol from the p-nitrophenyl phosphate substrate. OD was measured at 405 nm using a Thermo Scientific™ Multiskan™ GO Microplate Spectrophotometer (Thermo Scientific™, USA). ALP activity values were normalized to the total protein content obtained from the same cell lysate and expressed as units per microgram of total protein. Total protein content was determined using the BCA Protein Assay Kit (EMD Millipore Company, Darmstadt, Germany). The absorbance of the reaction product was measured at 562 nm.

The amount of mineralized matrix deposited onto the scaffolds was assessed using a Calcium Colorimetric Assay Kit (Biovision, Inc., USA). We measured the intensity of the stable purple colored complexes, which were directly proportional to the calcium concentration of the samples, at 575 nm using a Thermo Scientific™ Multiskan™ GO Microplate Spectrophotometer (Thermo Scientific™, USA).

2.10 qRT-PCR

The expression levels of osteogenic- and angiogenic-related genes were assessed using quantitative real time-polymerase chain reaction (qRT-PCR). Total RNA was extracted from cells seeded on the scaffolds using QIAzol lysis reagent (Qiagen, 79306). cDNA was synthesized by a cDNA kit (Takara: P3-T7) according to the manufacturer's instructions. Duplicate qRT-PCR reactions were performed with the SYBR Green Master Mix (Takara, Q3-PA33) with a real-time PCR system (Applied Biosystems Life Technologies, Inc., ABI StepOnePlus) and analyzed with StepOne software (Applied Biosystems, version 2.1). Three independent biological replicates were analyzed for each sample. The expression level of target genes was normalized to *β-actin* as the reference gene. Analysis was performed by the comparative ΔΔCT method. Primers are listed in Table 1.

Table 1 Description of primers used in qRT-PCR

Alp	F: 5' GCACAACATCAAGGACATCG 3'
	R: 5'TCAGTGCGGTTCCAGACATA 3'
Runx2	F: 5'GGACGAGGCAAGAGTTTCAC 3'
	R: 5'GAGGCGGTCAGAGAACAAAC 3'
Ocn	F: 5' GAGGGCAGTAAGGTGGTGAA 3'
	R: 5' GTCCGCTAGCTCGTCACAAT 3'
CD31	F: 5' TACACTTATTTATGAACCAGCCCT 3'
	R: 5' TCTGCACACCCAACATTAACA 3'
CD133	F: 5' TGCTGACCCTCTGAATCTG 3'
	R: 5' ATACATCCTCTGAATCCATCCTG 3'
Kdr	F: 5' CCCAGAAATGTACCAAACCA 3'
	R: 5' ACTTCCTCTTCCTCCATACAG 3'
β-actin	F: 5' CTATGTTGCCCTAGACTTCG 3'
	R: 5' AGGTCTTTACGGATGTCAAC 3'

2.11 Western blot analysis

We performed Western blot analysis to investigate the expression level of HIF-1α and the VEGF protein. Total protein was extracted by using lysis buffer (50 mM Tris-HCl, 150 mM NaCl, 1 mM EDTA, 1% NP-40, and 1% SDS) that contained 1 mM phenylmethylsulphonyl fluoride (PMSF) and phosphatase inhibitor cocktail, then centrifuged 15 min in 12000 rpm at 4℃, finally the concentration of the protein in lysate was measured by BCA kit. A total of 30 μg of proteins from each sample were separated on 10% polyacrylamide gels and transferred onto the PVDF membrane (wet transfer method, 12 V, and 12–14 h). PVDF was blocked with 5% milk for 2 h at room temperature under agitation. The membranes were incubated with the following primary antibodies: monoclonal anti-HIF-1 (ab-1, Abcam, 1:1000), monoclonal anti-VEGF antibody (ab1316, Abcam, 1:1000), and GAPDH (1:10000) overnight at 4 °C. The membranes were subsequently incubated with goat polyclonal secondary antibody HRP-conjugated secondary antibody (ab6789, Abcam, 1:5000) for 2 h at room temperature. The protein bands were visualized by using the SuperSignal West Femto Maximum Sensitivity Substrate (Thermo Fisher Scientific, Australia) and exposed on X-ray films (Fujifilm, Australia).

2.12 Super-paramagnetic iron oxide (SPIO) labeling

We labeled ADMSCs with super-paramagnetic iron oxide (SPIO) nanoparticles prior to implantation. ADSCs were incubated with serum-free culture medium that contained a mixture of SPIO (100 μg/mL) and protamine sulfate (45 μg/mL) for 2 h at 37 °C. Next, we added 20% FBS, 1% L-glutamine, and 1% penicillin/streptomycin to the cells. The cells were incubated for 48 h. Prussian blue staining was performed for cell visualization. Tissue sections were deparaffinized, rehydrated, and incubated in hydrochloride/potassium ferrocyanide (1:1 ratio) for 10 min. After washing, the samples were incubated with Pararosaniline stain for 5 min, and visualized by a light microscope (Olympus, Japan).

2.13 Animal study

In this study, 24 healthy male Wistar rats that weighed approximately 250 g were used as animal models. All experimental procedures that involved animals were performed in accordance with the standard operating procedures approved by the Institutional Animal Care and Ethics Committee of Royan institute. All animals were anesthetized by intraperitoneal injections of a mixture of ketamine–hydrochloric acid (HCl) [64 mg/mL]/xylazine [3.6 mg/mL] for a total dose of 0.2 mL/100 g body weight). We used a trephine drill to create two critical-sized defects (5 mm) in the calvarias of each animal. In each animal, the prepared constructs (5 mm diameter × 2 mm thick) were implanted in one defect, whereas the other defect was left empty (control). The 24 rats were randomly divided into four experimental groups included a cell-free DMOG-negative scaffold ($n = 6$), cell-free DMOG-positive scaffold ($n = 6$), cell-seeded DMOG-negative scaffold ($n = 6$), and cell-seeded DMOG-positive scaffold ($n = 6$). Post-operative analgesia and antibiotic therapy were then provided by subcutaneous (SC) administration of 1 mg/kg Meloxicam (Razak, Iran) and enrofloxacin (Irfan, Iran) for 3 days, respectively. All animals received humane care in compliance with the Guide for Care and Use of Laboratory Animals published by the National Institutes of Health (NIH Publication No. 85-23, revised 1985).The animals were euthanized 6 weeks post-implantation (WPI). The calvarias were harvested and used for histological analysis.

2.14 Histological analysis

Calvarias from all experimental groups were fixed in 10% formalin, followed by decalcification in nitric acid. Decalcified tissues were embedded in paraffin, cut into 6 μm sections, then stained with hematoxylin and eosin (H&E) and Masson's trichrome (MT).

2.15 Immunohistochemistry (IHC) analysis

Immunohistochemistry (IHC) was performed to assess the expressions of osteocalcin (OCN), RUNX2, and KDR (VEGFR2) proteins. Histological slides were treated with citrate buffer (pH 6) at 65 °C for antigen retrieval and blocked with goat serum for 2 h at 37 °C. Then, they were incubated with primary antibodies OCN (bs-4917R),

RUNX2 (orb10256), and KDR (ab2349) at 4 °C overnight. Samples were subsequently incubated with horseradish peroxidase (HRP)-labeled secondary antibody. Antibody complexes were observed after the addition of a buffered diaminobenzidine (DAB) solution. The sections were counterstained with hematoxylin and visualized by a light microscope (Olympus, Japan).

2.16 Histomorphometry

The amount of bone formation was quantitatively assessed using Image-Pro® Plus version 6.0 (Media Cybernetics, Silver Spring, MD, USA). A rectangular region of interest (10 non-overlapping areas) was set around the defect site within the microscopic images of the section. The area percentage of newly-formed bone was quantitatively measured with respect to the selected area for each section separately.

2.17 Statistical analyses

Statistical analyses were carried out on datasets that consisted of at least three independent experiments. We used one-way ANOVA with Tukey's multiple comparison tests, which compared more than two groups with SPSS software (version 16). All data are expressed as mean ± SD.

3 Results

3.1 Physical characteristics of fabricated scaffolds

We assessed the physical characteristics of the fabricated 3D scaffolds by examining their morphology, porosity, pore size, and mechanical properties. Fig. 1a,b shows SEM micrographs of the scaffolds with and without DMOG. The DMOG-negative scaffold showed a porous structure. Thin walls with a rather smooth surface separated the pores. Incorporation of DMOG, however, led to a scaffold with increased roughness and thicker pore walls.

Liquid displacement analysis showed an average porosity of 66.0919 ± 0.8128 for DMOG-negative scaffolds, whereas porosity decreased to 51.1905 ± 1.6836 for DMOG-positive scaffolds (Table 2). SEM images revealed that incorporation of DMOG in the TCP/alginate/gelatin scaffold led to decreased pore size of 147.0649 ± 36.1565 for DMOG-negative scaffolds to 105.6956 ± 23.1109 for DMOG-positive scaffolds. We observed an appropriate interconnected pore structure in both types of scaffolds.

Figure 1c shows compressive stress-strain curves for both DMOG-positive and negative scaffolds. Both scaffolds showed the mechanical behavior of porous materials with the initial linear-elastic region. Young's modulus was 0.465 ± 0.0235 MPa for the DMOG-negative scaffolds and 0.853 ± 0.0608 MPa for the DMOG-positive scaffolds. Young's modulus increased in scaffolds that contained DMOG compared to DMOG-negative scaffolds. Table 2 summarizes the physical properties of the fabricated scaffolds.

3.2 Dimethyloxalylglycine (DMOG) release

Figure 1d shows the cumulative DMOG release of phosphate buffer from the spongy scaffold. DMOG kinetic release profile showed that scaffolds released DMOG in a sustainable manner over 12 days. There was a burst release in the first two days of approximately 35% of the total DMOG followed by a slower release rate. By 12 days, 70% of the total DMOG concentration had been released.

3.3 Cell attachment and viability

Attachment of ADMSCs to both scaffolds was explored by SEM and H&E staining. H&E staining showed the presence of ADMSCs within the scaffolds (Fig. 2a, b). SEM micrographs indicated that ADMSCs attached to both scaffolds after 7 days (Fig. 2c, d). In order to determine whether the fabricated scaffolds had any toxic effects on ADMSCs, we performed the MTT assay on days 3 and 7. Fig. 2e shows that the viability of ADMSCs did not differ among the groups. The number of cells increased after 7 days in a similar way in all DMOG-negative, and positive scaffolds, as well as in the control group.

3.4 In vitro osteogenic activity

We evaluated osteogenic potential of both DMOG-positive and negative constructs by assessing the ALP activity, calcium content, and expression levels of osteogenic related genes at different time points (days 7 and 14). The level of ALP activity was higher in DMOG-positive compared to DMOG-negative constructs at day 7, but there was no significant difference between the two groups (Fig. 3a). After 14 days, ALP activity increased in both constructs. This was a significant increase in DMOG-positive scaffolds.

Figure 3b shows the amount of calcium deposition on spongy scaffolds after 7 and 14 days. Calcium content enhanced by increasing the experiment time to 14 days in both DMOG-positive and negative groups. There was a higher degree of calcium observed in the DMOG-positive construct compared to DMOG-negative construct at both time points.

The expression level of osteogenic-related genes was also assessed by qRT-PCR (Fig. 3c-e). Gene expression level of *Runx2*, an early stage osteogenic marker, considerably up-regulated in the DMOG-negative scaffold at days 7 and 14 compared to the DMOG-positive group.

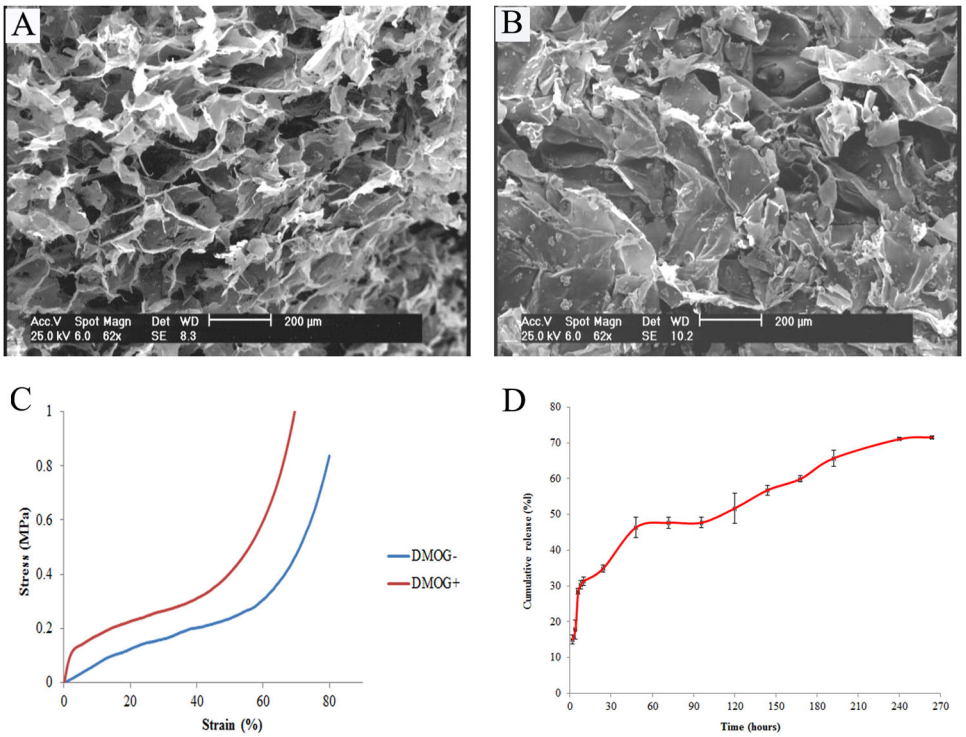

Fig. 1 Scaffold properties. Scanning electron microscopy (SEM) images of **a** dimethyloxalylglycine (DMOG)-negative and **b** DMOG-positive scaffolds. **c** Compressive stress-strain curve shows higher resistance of the scaffold to the failure. **d** Sustainable DMOG release profile over 12 days

Table 2 Calculated physical properties of the fabricated scaffolds

	Porosity (%)	Pore size (µm)	Yang module (MPa)
DMOG+	51.1905 ± 1.6836	105.6956 ± 23.1109	0.853 ± 0.0608
DMOG−	66.0919 ± 0.8128	147.0649 ± 36.1565	0.465 ± 0.0235

*R*unx*2* downregulated in the DMOG-positive group over time.

In contrast, *Alp* increased in the DMOG-positive group compared with the negative group at each time point. We observed a significant reduction in both groups at day 14. Similarly, there was a higher level of *Ocn* expression in the DMOG-positive scaffold compared to the DMOG-negative scaffold ($p \leq 0.05$), particularly at day 14.

3.5 Angiogenesis evaluation

We performed Western blot analysis of the stimulatory effect of DMOG on angiogenesis and qRT-PCR for angiogenic factors. Fig. 4 a, b show expressions of HIF-1α and VEGF at the protein level after 3 and 7 days. Expression of HIF-1α markedly enhanced in both DMOG-positive and negative groups compared to the control groups. However, there were no significant differences between DMOG-positive and negative scaffolds at both time points. VEGF upregulated in the experimental groups relative to the control group. However, cells seeded on the scaffolds that contained DMOG expressed VEGF protein higher than DMOG-negative and control groups at day 7.

Expressions of angiogenic-related genes that included *CD31*, *Kdr*, and *CD133* are shown in Fig. 4c-e. Interestingly, the DMOG-positive group had substantial enhancement of all three genes compared to the DMOG-negative group at day 7. However, this difference was only statistically significant for *CD31* and *CD133*. After 14 days, we observed down-regulation of *CD31*, *Kdr*, and *CD133* for both groups. The DMOG-positive group had a higher expression level compared to the negative group.

3.6 Computed tomography (CT) scan analysis

CT scan analysis was performed for all groups 6 WPI. The defect size reduced in all groups compared to the untreated group (Fig. 5). We observed a smaller defect size in all DMOG-positive scaffolds of the cell-seeded and unseeded groups compared to DMOG-negative scaffolds.

3.7 Histopathology and histomorphometry

We performed histological analysis (H&E and MT staining) of the harvested calvaria from all experimental groups at 6 WPI. H&E staining showed that the periosteum covered the defect site in the untreated group with no fibrous tissue formation after 6 weeks. In contrast, the construct was integrated to the host tissue on both sides of the defect site. Additionally, a large number of host cells infiltrated into the

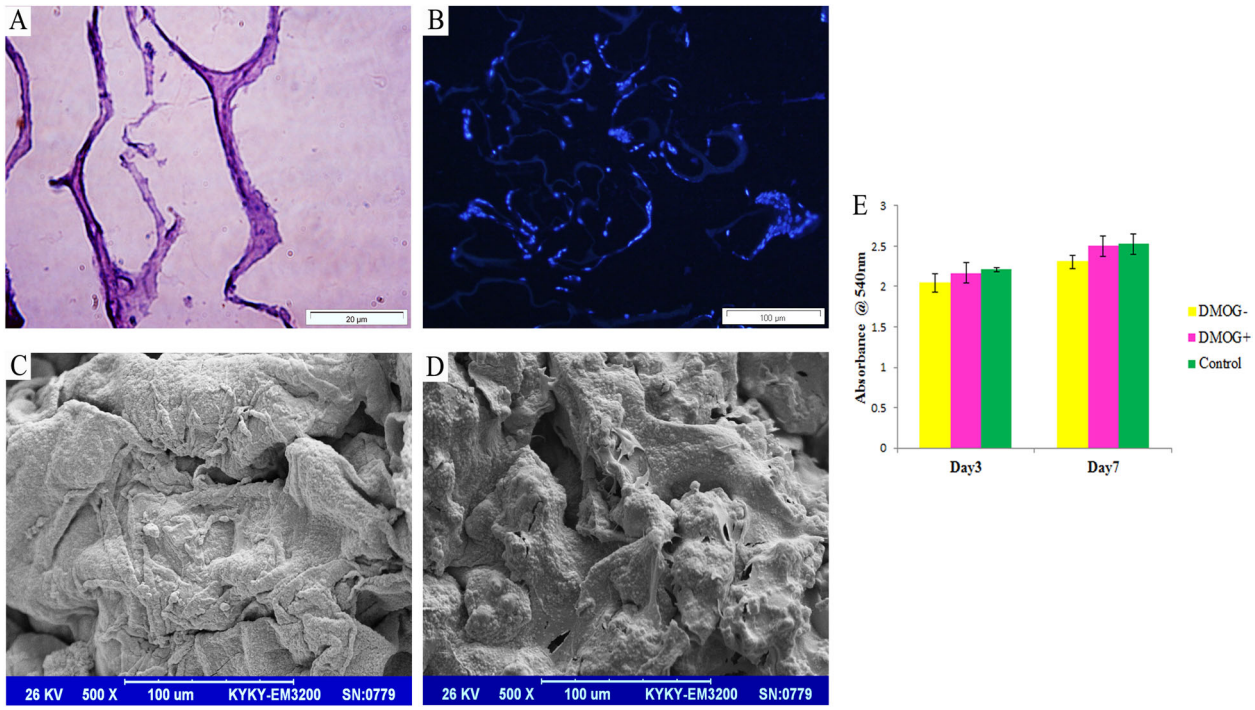

Fig. 2 Cell attachment and viability. **a** The presence of adipose derived mesenchymal stem cells (ADMSCs) on spongy scaffolds was confirmed by H&E staining. **b** Nuclei counterstained with DAPI. **c** Scanning electron microscopy (SEM) image of ADMSCs seeded onto dimethyloxalylglycine (DMOG) negative and **d** DMOG-positive scaffolds. **e** Histogram represents the viability of ADMSCs on spongy scaffolds with or without DMOG. Optical density (OD) of ADMSCs seeded on the scaffold did not show any significant difference between the scaffolds and control group. Data are presented as means ± SD ($n = 3$) *$p < 0.05$

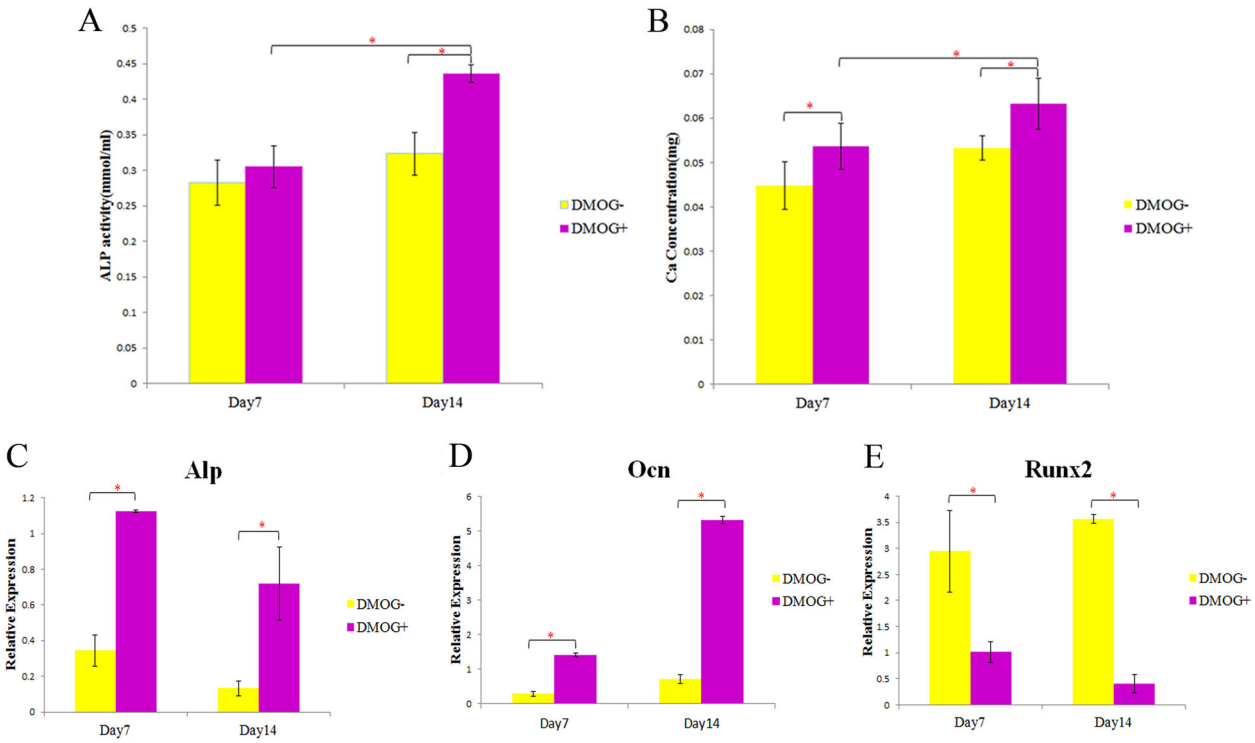

Fig. 3 Osteogenic activity of adipose derived mesenchymal stem cell (ADMSC)-seeded constructs. Histograms show **a** ALP activity and **b** calcium content after 7 and 14 days. qRT-PCR analysis was performed for C *Runx2*, **d** *Alp*, and **e** *Ocn* osteogenic markers expressed by ADMSCs on dimethyloxalylglycine (DMOG) positive and negative scaffolds at days 7 and 14. Higher expression levels of *Ocn* and *Alp* as well as down-regulation of *Runx2* were detected in the DMOG-positive group. Data are presented as means ± SD ($n = 3$). *$p < 0.05$

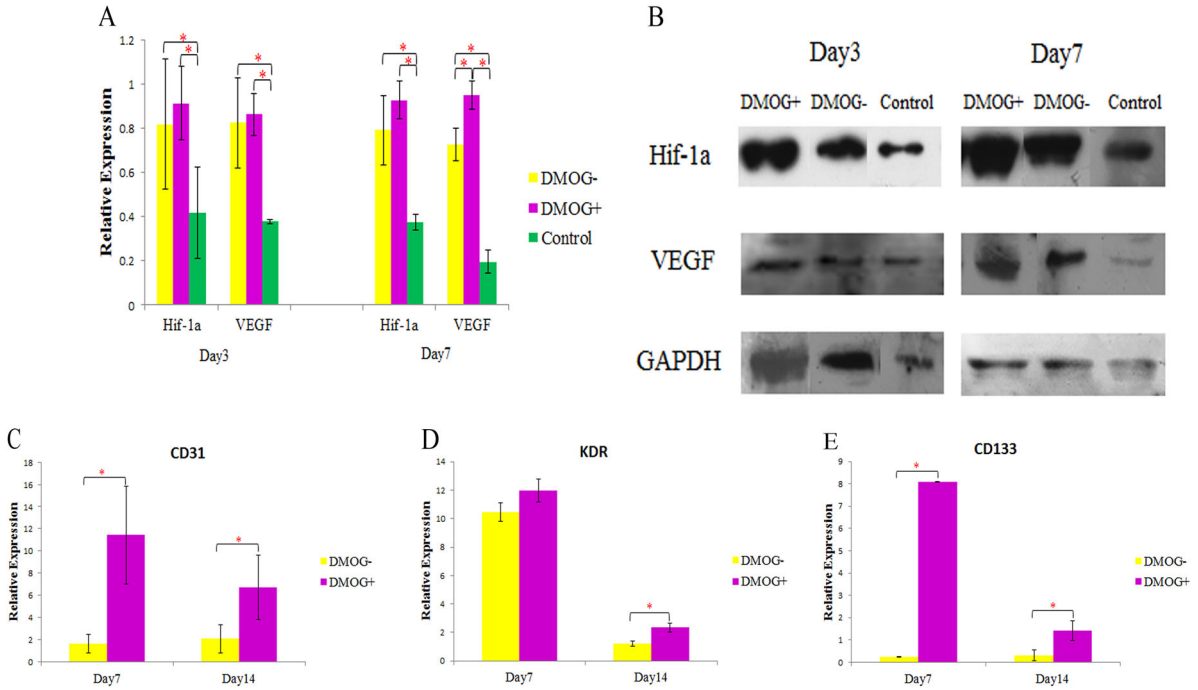

Fig. 4 Angiogenic activity. Histogram **a** shows quantitative analysis of hypoxia-inducible factor-1α (HIF-1α) and VEGF expression levels and **b** band density analysis of HIF-1α and VEGF by Western blot after days 3 and 7. Real time-PCR analysis of **c** *CD31*, **d** *Kdr*, and **e** *CD133* genes showed enhanced expression levels in the dimethyloxalylglycine (DMOG)-positive group compared to the DMOG-negative group after 7 and 14 days. Data are presented as means ± SD ($n = 3$). *$p < 0.05$

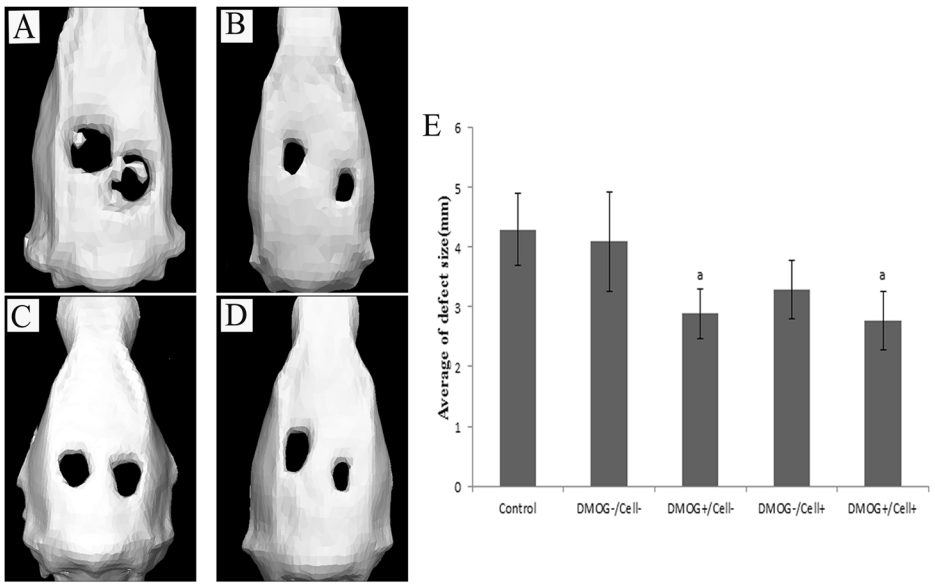

Fig. 5 Computed tomography (CT) scan imaging. CT scan of cell-free **a** dimethyloxalylglycine (DMOG) negative, **b** cell-free DMOG-positive, **c** cell-seeded DMOG-negative, and **d** cell-seeded DMOG-positive constructs. Right defects filled by the constructs and left defects were empty. **e** Histogram shows the size of restored calvaria defects 6 weeks post-implantation (WPI). Data are presented as means ± SD ($n = 3$). a shows a statistically significant difference compared to control group ($p < 0.05$)

cell-free DMOG-positive and negative scaffolds at the defect area (Fig. 6). Histological analysis indicated that the scaffolds partially degraded in all treated group and remnants of all scaffolds were present at the defect site. The amount of scaffold residue was higher in the cell-free groups. New bone formation occurred within the implantation site in the treated groups, yet the density of newly-formed bone differed among all groups. There was a higher degree of new bone in the defects treated with cell-seeded DMOG-positive construct followed by cell-seeded DMOG-negative, cell-free DMOG-positive, and cell-free DMOG-negative constructs. The cell-free DMOG-positive

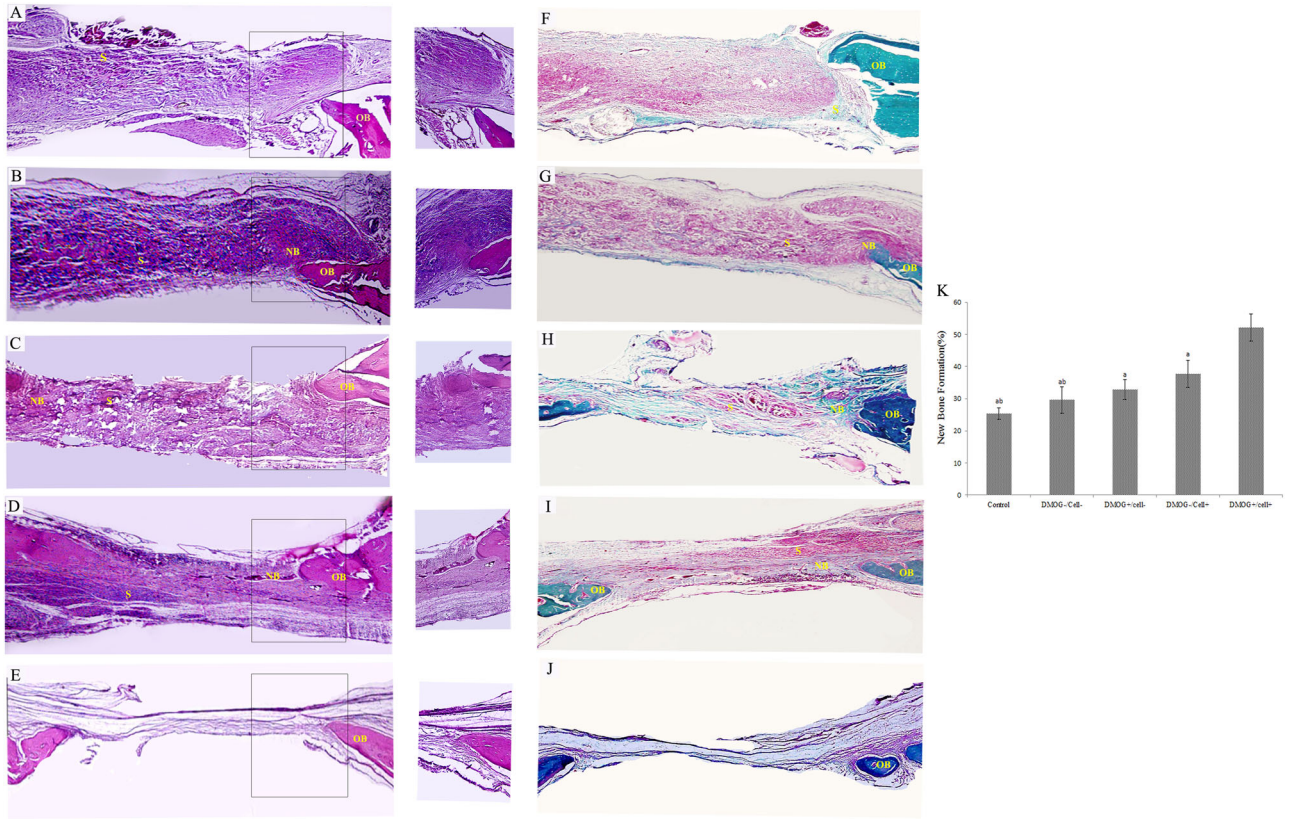

Fig. 6 Histological analysis. Hematoxylin and eosin (H&E) and Masson's trichrome (MT) staining of **a**, **f** cell-free dimethyloxalylglycine (DMOG)-negative, **b**, **g** cell-free DMOG-positive, **c**, **h** cell-seeded DMOG, and **d**, **i** cell-seeded DMOG-positive constructs, and the **e**, **j** control group without any implantation 6 weeks post-surgery. **k** Histogram shows the degree of new bone formation quantitatively analyzed by Image Pro Plus software. OB Old bone, NB New bone, and S Scaffold residue. (Magnification for all pictures: 40 ×). Data are presented as means ± SD ($n = 6$). a and b show a statistically significant differences compared to control group and cell free DMOG-negative group, respectively ($p < 0.05$)

scaffolds and cell-seeded DMOG-negative construct exhibited similar degrees of newly-formed bone tissue.

Figure 7 shows IHC staining of decalcified calvaria for osteogenic (OCN, RUNX2) and angiogenic (KDR) markers. OCN highly expressed in the cell-loaded scaffold that contained DMOG, while low expression level of the same marker was observed in the cell-free DMOG-negative group (Fig. 7Ba). There were no significant differences among the cell-seeded DMOG-positive, cell-seeded DMOG-negative, and cell-free DMOG-positive groups. The cell-seeded DMOG-positive group showed a significant increase in RUNX2 (Fig. 7Bb) compared to the other groups. The amount of RUNX2 expression level was similar between the cell-seeded DMOG-negative and cell-free DMOG-positive groups.

We observed the highest expression level of KDR in the cell-seeded scaffold with DMOG amongst all of the treated groups (Fig. 7Bc). Cell-seeded DMOG-negative and cell-free DMOG-positive groups also expressed the same levels of the KDR protein.

4 Discussion

HIF-1α signaling is considered to be a crucial upstream regulator of blood vessel formation [28, 29]. In addition, HIF-1α activates ECs to generate specified microenvironments that encourage osteoprogenitor recruitment and osteogenic activity [30–32]. DMOG is a cell-permeable prolyl-4-hydroxylase inhibitor, which up-regulates the expression level of HIF-1α protein post-transcriptionally under normoxic conditions [33–35]. Hence, in this study, we have used a three-component spongy scaffold, alginate-gelatin-tricalcium phosphate, as a novel vehicle for DMOG delivery. Next, we explored the regenerative potential of fabricated scaffolds in critical-sized calvarial defects in a rat model (Fig. 8).

Analysis of physical properties of fabricated scaffolds revealed that incorporation of DMOG in alginate-gelatin-tricalcium phosphate led to a distinguished microstructure with thickened pore walls and boosted surface roughness. A comparison of DMOG-negative and positive scaffolds confirmed the higher mechanical strength in the DMOG-

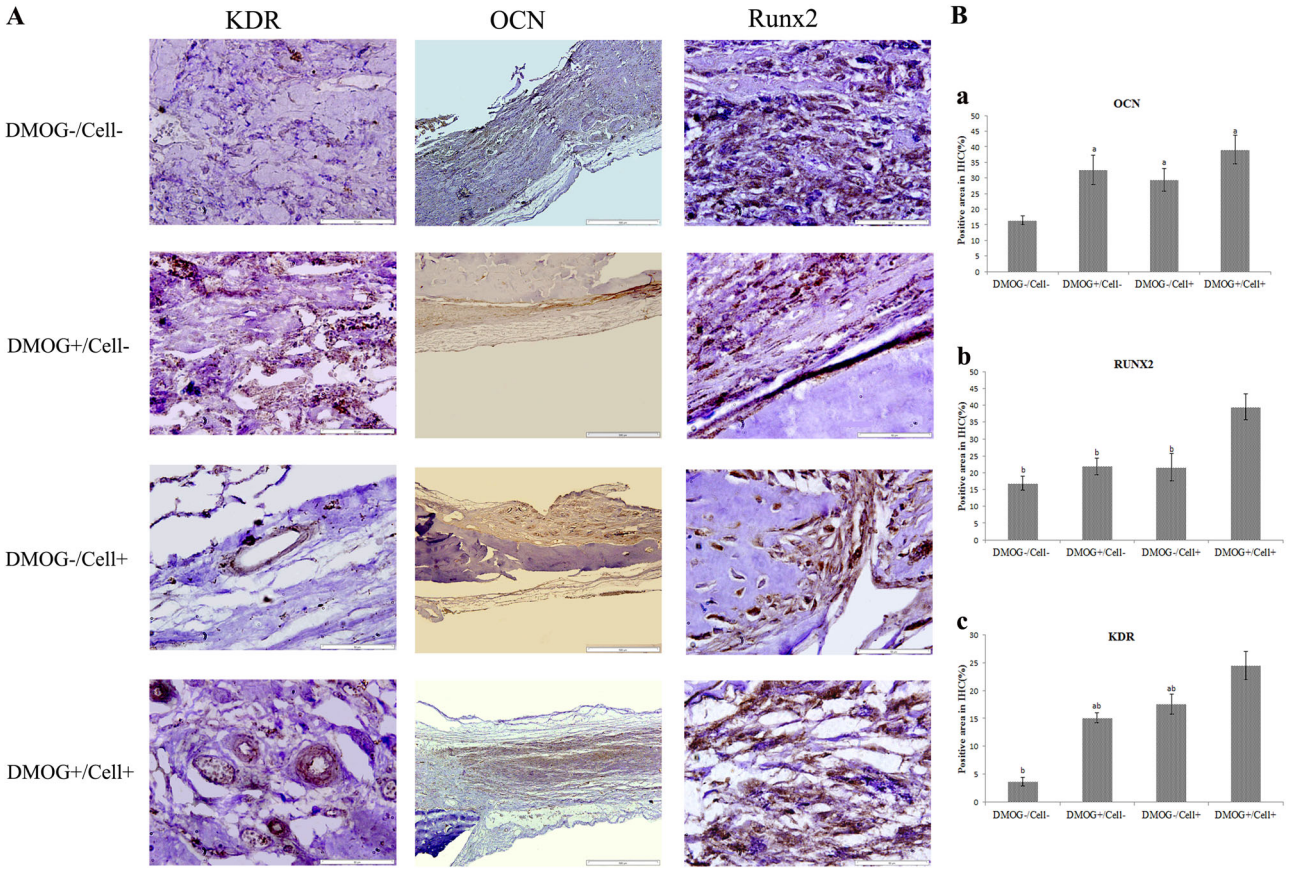

Fig. 7 Immunohistochemistry (IHC) analysis. IHC staining **a** shows increased expressions of OCN, RUNX2, and KDR in cell-seeded dimethyloxalylglycine (DMOG) positive groups compared to the other groups. Histograms **b** represent the quantitative analysis of OSN **a**, RUNX2 **b**, and KDR **c** performed by Image Pro Plus software. Data are presented as means ± SD ($n = 3$). a and b show a statistically significant differences compared to cell free DMOG-negative group and cell-seeded DMOG-positive group, respectively ($p < 0.05$)

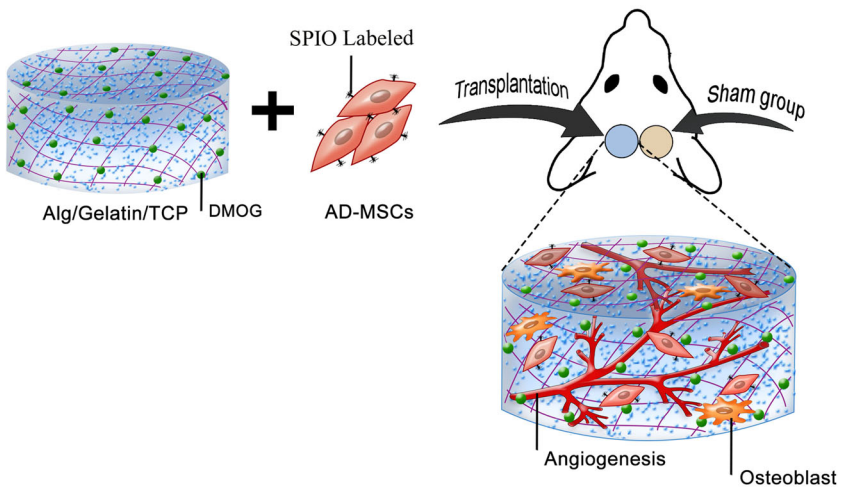

Fig. 8 Schematic representation of study design. Spongy scaffold that included sodium alginate-gelatin-β-tricalcium phosphate and DMOG was fabricated and subsequently SPIO-labeled ADMSCs seeded onto the scaffolds. After in vitro characterization, 3D constructs were implanted in calvarial defects in a rat model

positive scaffold according to the compressive stress-strain curve. There was low mechanical strength yet adequate elastic modulus (0.853 ± 0.0608 MPa) of the DMOG scaffold While Tan et al. reported an elastic modulus of 0.17-0.56 MPa for alginate/calcium phosphate [36].

The results obtained from the release profile indicated that the scaffold delivered DMOG in a sustainable manner as 70% of the drug was released over 12 days. The rate of DMOG release decreased compared to previous studies that reported total DMOG release up to day 6 [20, 37]. An initial blood supply must be provided during the early days post-

implantation until the newly-formed blood vessels of the host tissue could begin to support the implanted construct. Lack of adequate vessels would result in insufficient oxygen and nutrition, and eventual cell death in the center of the construct. Hence, this time determines the success or failure of a transplant [38–40]. Therefore, our construct that delivered DMOG over a long period of time could accelerate angiogenesis and avoid cell death until connected to the host vascular network. We could increase the efficiency of DMOG loading as this parameter was reported to be relatively low in previous studies [37, 41].

Biocompatibility is a critical parameter for biological scaffolds [42]. According to the MTT results, DMOG (1 mg/ml) did not have any toxic effect on ADMSCs. The ADMSCs greatly attached to the surface of the spongy scaffolds as observed by H&E and SEM. We previously demonstrated that the spongy scaffold which consisted of alginate-gelatin-β tricalcium phosphate had the capability to promote cellular attachment and proliferation [27].

We explored the osteogenic potential of the DMOG-containing scaffold under in vitro conditions. The results obtained from analysis of ALP activity showed that the DMOG-positive scaffold had a higher level of ALP activity compared to the DMOG-negative scaffold. qRT-PCR confirmed the level of *Alp* in the DMOG-containing scaffold. Calcium deposition, as an indication of mineralization, also increased in the presence of DMOG, which was consistent with ALP activity results. These data confirmed the effect of DMOG on the osteogenic differentiation of ADMSCs. A previous study showed that DMOG resulted in higher ALP activity and osteogenic related genes [43].

We sought to precisely address how DMOG affected the expressions of osteogenic-related genes. qRT-PCR analysis of *Runx2* and *Ocn* have shown that *Runx2* expression significantly increased in DMOG-negative scaffolds compared to the DMOG-positive group. *Runx2*, as an early marker for bone differentiation, is expected to up-regulate during the first days of the osteogenic process. Therefore, DMOG appeared to accelerate the process of osteoblastic differentiation such that *Runx2* up-regulated before 7 days in the DMOG-positive group. Accordingly, ADMSCs loaded onto the DMOG-positive scaffold significantly expressed *Ocn* compared to the DMOG-free group. Since OCN is a late marker of osteogenesis, it seems that the DMOG-negative scaffold would only have the capability to drive osteogenic differentiation during the early stages and would need another stimulus to continue this process. Therefore, the significant differences in *Ocn* expression between DMOG-negative and positive groups might be attributed to the DMOG delivery that promoted osteogenic activity. Improved physical characteristics of the scaffolds that contained DMOG, such as mechanical strength, most likely resulted in boosted osteoblastic differentiation as confirmed by previous studies [44, 45].

The expression of angiogenic genes *Kdr, CD31* and *CD133* were shown by qRT-PCR analysis. As expected, the DMOG-containing scaffold induced the expression of all vascular markers, which indicated that DMOG could mimic hypoxia. This, in turn, led to up-regulation of angiogenesis markers. Surprisingly, *Kdr* highly expressed in ADMSCs that were loaded onto a DMOG-free scaffold. The elevated expression level of *Kdr* in this group might be related to either the presence of EPCs in the cultured cell population or the activation of another hypoxia pathway by the spongy scaffold. *CD31* and *CD133*, which are involved in the elongation of the vascular network, did not up-regulate. This finding suggested that scaffold does not solely have the capability to fulfill vascular differentiation in the absence of DMOG. To clearly show that DMOG affected angiogenesis, we evaluated the expressions of the HIF-1α and VEGF proteins. Both scaffolds expressed HIF-1α, yet only the DMOG-positive scaffold had the ability to stimulate VEGF expression, which was consistent with the literature [37]. Since the fabricated scaffold has a spongy form, it provides the hypoxic condition in the center of scaffold. Therefore, hypoxia would increase the HIF expression level in both scaffolds. Moreover, it has been previously reported that DMOG stabilize the HIF-1 protein [46]. It is more probably the more stabilized form of HIF-1 in the presence of DMOG resulted in higher VEGF level and angiogenesis markers in our study, although we could not observed the difference in expression level of HIF between groups. These results, combined with qRT-PCR results, confirmed the essential role of DMOG in vascular network elongation and stability.

We further explored the regenerative ability of fabricated scaffolds following implantation into rat calvarial defects. Our histomorphometry and IHC results showed a superior osteogenesis in cell-seeded DMOG-positive group compared to the other groups. SPIO labeled cells were tracked in the defect site at 6 WPI. This demonstrated contribution of the exogenous cells to bone regeneration (Supplementary F1). We observed that considerable cell numbers recruited to the defects that were treated with both cell-free positive and negative DMOG scaffolds. Interestingly, we observed no significant difference in terms of bone mineralization between the defects treated with cell-free DMOG-positive and cell-loaded DMOG-negative constructs, which indicated the effectiveness of DMOG in osteogenesis. It should be taken into consideration that the defects were not fully restored during the experimental time (6 weeks). Therefore, long-term follow up would be required. Similar studies reported the same results on rat calvaria defects over 6–8 weeks [47–49].

Our results have demonstrated that DMOG delivery with cell-loaded scaffold can support osteogenesis and

angiogenesis both in vitro and in vivo. The cell-free scaffold that contained DMOG can be utilized as a bone tissue substitute since it efficiently rendered osteogenesis in the bone defect. Further investigations are needed to achieve better restorative outcomes through improvement of mechanical properties and release time.

Acknowledgements The present research was financially supported by Royan Institute for Stem Cell Biology and Technology. We thank Ms. Fatemeh Safari and Mr. Mohammad Hossein Ghanian for their help.

Compliance with ethical standards

Conflict of interest The authors declare that they have no conflict of interest.

Publisher's note: Springer Nature remains neutral with regard to jurisdictional claims in published maps and institutional affiliations.

References

1. Arvidson K, Abdallah BM, Applegate LA, Baldini N, Cenni E, Gomez-Barrena E. et al. Bone regeneration and stem cells. J Cell Mol Med. 2011;15:718–46. https://doi.org/10.1111/j.1582-4934.2010.01224.x.
2. Khan SN, Cammisa FP Jr., Sandhu HS, Diwan AD, Girardi FP, Lane JM. The biology of bone grafting. J Am Acad Orthop Surg. 2005;13:77–86.
3. Frohlich M, Grayson WL, Wan LQ, Marolt D, Drobnic M, Vunjak-Novakovic G. Tissue engineered bone grafts: biological requirements, tissue culture and clinical relevance. Curr Stem Cell Res Ther. 2008;3:254–64.
4. Lokmic Z, Mitchell GM. Engineering the microcirculation. Tissue Eng Part B Rev. 2008;14:87–103. https://doi.org/10.1089/teb.2007.0299.
5. Kaigler D, Wang Z, Horger K, Mooney DJ, Krebsbach PH. VEGF scaffolds enhance angiogenesis and bone regeneration in irradiated osseous defects. J Bone Miner Res. 2006;21:735–44. https://doi.org/10.1359/jbmr.060120.
6. Khojasteh A, Fahimipour F, Eslaminejad MB, Jafarian M, Jahangir S, Bastami F. et al. Development of PLGA-coated beta-TCP scaffolds containing VEGF for bone tissue engineering. Mater Sci Eng C Mater Biol Appl. 2016;69:780–8. https://doi.org/10.1016/j.msec.2016.07.011.
7. Leach JK, Kaigler D, Wang Z, Krebsbach PH, Mooney DJ. Coating of VEGF-releasing scaffolds with bioactive glass for angiogenesis and bone regeneration. Biomaterials. 2006;27:3249–55. https://doi.org/10.1016/j.biomaterials.2006.01.033.
8. Chen RR, Silva EA, Yuen WW, Mooney DJ. Spatio-temporal VEGF and PDGF delivery patterns blood vessel formation and maturation. Pharm Res. 2007;24:258–64. https://doi.org/10.1007/s11095-006-9173-4.
9. Alsop AT, Pence JC, Weisgerber DW, Harley BAC, Bailey RC. Photopatterning of vascular endothelial growth factor within collagen-glycosaminoglycan scaffolds can induce a spatially confined response in human umbilical vein endothelial cells. Acta Biomater. 2014;10:4715–22. https://doi.org/10.1016/j.actbio.2014.07.002.
10. Fan L, Li J, Yu Z, Dang X, Wang K. The hypoxia-inducible factor pathway, prolyl hydroxylase domain protein inhibitors, and their roles in bone repair and regeneration. Biomed Res Int. 2014;2014:239356. https://doi.org/10.1155/2014/239356.
11. Wang Y, Wan C, Gilbert SR, Clemens TL. Oxygen sensing and osteogenesis. Ann N Y Acad Sci. 2007;1117:1–11. https://doi.org/10.1196/annals.1402.049.
12. Keith B, Johnson RS, Simon MCHIF1alpha. and HIF2alpha: sibling rivalry in hypoxic tumour growth and progression. Nat Rev Cancer. 2011;12:9–22. https://doi.org/10.1038/nrc3183.
13. Wilson WR, Hay MP. Targeting hypoxia in cancer therapy. Nat Rev Cancer. 2011;11:393–410. https://doi.org/10.1038/nrc3064.
14. Jaakkola P, Mole DR, Tian YM, Wilson MI, Gielbert J, Gaskell SJ. et al. Targeting of HIF-alpha to the von Hippel-Lindau ubiquitylation complex by O2-regulated prolyl hydroxylation. Science. 2001;292:468–72. https://doi.org/10.1126/science.1059796.
15. Berra E, Benizri E, Ginouves A, Volmat V, Roux D, Pouyssegur J. HIF prolyl-hydroxylase 2 is the key oxygen sensor setting low steady-state levels of HIF-1alpha in normoxia. EMBO J. 2003;22:4082–90. https://doi.org/10.1093/emboj/cdg392.
16. Mole DR, Schlemminger I, McNeill LA, Hewitson KS, Pugh CW, Ratcliffe PJ, et al. 2-oxoglutarate analogue inhibitors of HIF prolyl hydroxylase. Bioorg Med Chem Lett. 2003;13:2677–80.
17. Holotnakova T, Ziegelhoffer A, Ohradanova A, Hulikova A, Novakova M, Kopacek J. et al. Induction of carbonic anhydrase IX by hypoxia and chemical disruption of oxygen sensing in rat fibroblasts and cardiomyocytes. Pflug Arch. 2008;456:323–37. https://doi.org/10.1007/s00424-007-0400-6.
18. Peng J, Lai ZG, Fang ZL, Xing S, Hui K, Hao C. et al.Dimethyloxalylglycine prevents bone loss in ovariectomized C57BL/6J mice through enhanced angiogenesis and osteogenesis. PLoS ONE. 2014;9:e112744. https://doi.org/10.1371/journal.pone.0112744.
19. Vogel S, Wottawa M, Farhat K, Zieseniss A, Schnelle M, Le-Huu S. et al.Prolyl hydroxylase domain (PHD) 2 affects cell migration and F-actin formation via RhoA/rho-associated kinase-dependent cofilin phosphorylation. J Biol Chem. 2010;285:33756–63.https://doi.org/10.1074/jbc.M110.132985.
20. Qi X, Liu Y, Ding ZY, Cao JQ, Huang JH, Zhang JY. et al. Synergistic effects of dimethyloxallyl glycine and recombinant human bone morphogenetic protein-2 on repair of critical-sized bone defects in rats. Sci Rep. 2017;7:42820. https://doi.org/10.1038/srep42820.
21. Oryan A, Kamali A, Moshiri A, Baghaban Eslaminejad M. Role of mesenchymal stem cells in bone regenerative medicine: what is the evidence?. Cells Tissues Organs. 2017;204:59–83. https://doi.org/10.1159/000469704.
22. Fu WL, Xiang Z, Huang FG, Gu ZP, Yu XX, Cen SQ. et al. Coculture of peripheral blood-derived mesenchymal stem cells and endothelial progenitor cells on strontium-doped calcium polyphosphate scaffolds to generate vascularized engineered bone. Tissue Eng Part A. 2015;21:948–59.https://doi.org/10.1089/ten.TEA.2014.0267.
23. Koob S, Torio-Padron N, Stark GB, Hannig C, Stankovic Z, Finkenzeller G. Bone formation and neovascularization mediated by mesenchymal stem cells and endothelial cells in critical-sized calvarial defects. Tissue Eng Part A. 2011;17:311–21. https://doi.org/10.1089/ten.TEA.2010.0338.
24. Strem BM, Hicok KC, Zhu M, Wulur I, Alfonso Z, Schreiber RE, et al. Multipotential differentiation of adipose tissue-derived stem cells. Keio J Med. 2005;54:132–41.
25. Baer PC, Geiger H. Adipose-derived mesenchymal stromal/stem cells: tissue localization, characterization, and heterogeneity. Stem Cells Int. 2012;2012:812693. https://doi.org/10.1155/2012/812693.
26. Rennerfeldt DA, Van Vliet KJ. Concise review: when colonies are not clones: evidence and implications of intracolony heterogeneity in mesenchymal. Stem Cells. 2016;34:1135–41. https://doi.org/10.1002/stem.2296.

27. Eslaminejad MB, Mirzadeh H, Mohamadi Y, Nickmahzar A. Bone differentiation of marrow-derived mesenchymal stem cells using beta-tricalcium phosphate-alginate-gelatin hybrid scaffolds. J Tissue Eng Regen Med. 2007;1:417–24. https://doi.org/10.1002/term.49.
28. Ceradini DJ, Kulkarni AR, Callaghan MJ, Tepper OM, Bastidas N, Kleinman ME. et al. Progenitor cell trafficking is regulated by hypoxic gradients through HIF-1 induction of SDF-1. Nat Med. 2004;10:858–64. https://doi.org/10.1038/nm1075.
29. Greijer AE, van der Groep P, Kemming D, Shvarts A, Semenza GL, Meijer GA. et al. Up-regulation of gene expression by hypoxia is mediated predominantly by hypoxia-inducible factor 1 (HIF-1). J Pathol. 2005;206:291–304. https://doi.org/10.1002/path.1778.
30. Kusumbe AP, Ramasamy SK, Adams RH. Coupling of angiogenesis and osteogenesis by a specific vessel subtype in bone. Nature. 2014;507:323–8. https://doi.org/10.1038/nature13145.
31. Riddle RC, Khatri R, Schipani E, Clemens TL. Role of hypoxia-inducible factor-1alpha in angiogenic-osteogenic coupling. J Mol Med (Berl). 2009;87:583–90. https://doi.org/10.1007/s00109-009-0477-9.
32. Wan C, Shao J, Gilbert SR, Riddle RC, Long F, Johnson RS. et al. Role of HIF-1alpha in skeletal development. Ann N Y Acad Sci. 2010;1192:322–6. https://doi.org/10.1111/j.1749-6632.2009.05238.x.
33. Asikainen TM, Ahmad A, Schneider BK, Ho WB, Arend M, Brenner M. et al. Stimulation of HIF-1alpha, HIF-2alpha, and VEGF by prolyl 4-hydroxylase inhibition in human lung endothelial and epithelial cells. Free Radic Biol Med. 2005;38:1002–13. https://doi.org/10.1016/j.freeradbiomed.2004.12.004.
34. Ding H, Gao YS, Wang Y, Hu C, Sun Y, Zhang C. Dimethyloxaloylglycine increases the bone healing capacity of adipose-derived stem cells by promoting osteogenic differentiation and angiogenic potential. Stem Cells Dev. 2014;23:990–1000. https://doi.org/10.1089/scd.2013.0486.
35. Rey S, Lee K, Wang CJ, Gupta K, Chen S, McMillan A. et al. Synergistic effect of HIF-1alpha gene therapy and HIF-1-activated bone marrow-derived angiogenic cells in a mouse model of limb ischemia. Proc Natl Acad Sci USA. 2009;106:20399–404. https://doi.org/10.1073/pnas.0911921106.
36. Tan R, Niu X, Gan S, Feng Q.Preparation and characterization of an injectable composite. J Mater Sci Mater Med. 2009;20:1245–53.https://doi.org/10.1007/s10856-009-3692-6.
37. Wu C, Zhou Y, Chang J, Xiao Y. Delivery of dimethyloxallyl glycine in mesoporous bioactive glass scaffolds to improve angiogenesis and osteogenesis of human bone marrow stromal cells. Acta Biomater. 2013;9:9159–68. https://doi.org/10.1016/j.actbio.2013.06.026.
38. Aronson J. Temporal and spatial increases in blood flow during distraction osteogenesis. Clin Orthop Relat Res. 1994;301:124–31.
39. Mooney DJ, Mikos AG. Growing new organs. Sci Am. 1999;280:60–5.
40. Yu H, VandeVord PJ, Mao L, Matthew HW, Wooley PH, Yang SY. Improved tissue-engineered bone regeneration by endothelial cell mediated vascularization. Biomaterials. 2009;30:508–17. https://doi.org/10.1016/j.biomaterials.2008.09.047.
41. Agis H, Hueber L, Pour Sadeghian N, Pensch M, Gruber R. In vitro release of dimethyloxaloylglycine and l-mimosine from bovine bone mineral. Arch Oral Biol. 2014;59:1024–31. https://doi.org/10.1016/j.archoralbio.2014.05.027.
42. Kim BS, Mooney DJ. Development of biocompatible synthetic extracellular matrices for tissue engineering. Trends Biotechnol. 1998;16:224–30.
43. Min Z, Shichang Z, Chen X, Yufang Z, Changqing Z. 3D-printed dimethyloxallyl glycine delivery scaffolds to improve angiogenesis and osteogenesis. Biomater Sci. 2015;3:1236–44. https://doi.org/10.1039/c5bm00132c.
44. Engler AJ, Sen S, Sweeney HL, Discher DE. Matrix elasticity directs stem cell lineage specification. Cell. 2006;126:677–89. https://doi.org/10.1016/j.cell.2006.06.044.
45. Tokuda EY, Leight JL, Anseth KS. Modulation of matrix elasticity with PEG hydrogels to study melanoma drug responsiveness. Biomaterials. 2014;35:4310–8. https://doi.org/10.1016/j.biomaterials.2014.01.063.
46. Jaakkola P, Mole DR, Tian Y-M, Wilson MI, Gielbert J, Gaskell SJ, et al. Targeting of HIF-α to the von Hippel-Lindau ubiquitylation complex by O_2- regulated prolyl hydroxylation. Science. 2001;292:468.
47. Blum JS, Barry MA, Mikos AG, Jansen JA. In vivo evaluation of gene therapy vectors in ex vivo-derived marrow stromal cells for bone regeneration in a rat critical-size calvarial defect model. Hum Gene Ther. 2003;14:1689–701. https://doi.org/10.1089/104303403322611719.
48. Cowan CM, Aghaloo T, Chou YF, Walder B, Zhang X, Soo C. et al. MicroCT evaluation of three-dimensional mineralization in response to BMP-2 doses in vitro and in critical sized rat calvarial defects. Tissue Eng. 2007;13:501–12. https://doi.org/10.1089/ten.2006.0141.
49. Yoon E, Dhar S, Chun DE, Gharibjanian NA, Evans GR. In vivo osteogenic potential of human adipose-derived stem cells/poly lactide-co-glycolic acid constructs for bone regeneration in a rat critical-sized calvarial defect model. Tissue Eng. 2007;13:619–27. https://doi.org/10.1089/ten.2006.0102.